The new very-small-angle neutron scattering spectrometer at Laboratoire Léon Brillouin

S. Désert,[a]* V. Thévenot,[a] J. Oberdisse[b] and A. Brûlet[a]

[a]Laboratoire Léon Brillouin, CEA Saclay, 91191 Gif-Yvette, France, and [b]Laboratoire des Colloïdes, Verres et Nanomatériaux, 34095 Montpellier, France. Correspondence e-mail: desert@drecam.cea.fr

The design and characteristics of the new very-small-angle neutron scattering spectrometer under construction at the Laboratoire Léon Brillouin are described. Its goal is to extend the range of scattering-vector magnitudes towards 2×10^{-4} Å^{-1}. The unique feature of this new spectrometer is a high-resolution two-dimensional image-plate detector sensitive to neutrons. The wavelength selection is achieved by a double-reflection supermirror monochromator and the collimator uses a novel multibeam design.

1. Introduction

More and more studies of large-scale objects (> 50 nm) are needed nowadays. The very-small-angle neutron scattering (VSANS) spectrometer (*très petits angles*, TPA) will be dedicated to the study of such nanostructures, usually found in aggregates, branched polymers, organized multi-component systems (such as vesicles), reinforced rubber, cell membranes in biology, clays, porous systems, alloys in metallurgy, and vortex lattices in supraconductors.

TPA has been developed to reach a scattering vector modulus q down to 2×10^{-4} Å^{-1} with $q = (4\pi/\lambda)\sin(\theta/2)$, where θ is the scattering angle and λ is the neutron wavelength. Such a small q value is lower than those obtained by classical small-angle scattering pinhole spectrometers in order to fill the gap between light scattering and classical small-angle neutron scattering (SANS). It is very different from the ultra small-angle neutron scattering spectrometers which can reach scattering vectors still one order of magnitude lower by using double-crystal monochromators (Bonse & Hart, 1965). The principles of TPA are the same as for classical SANS spectrometers: pinhole collimation but with very small apertures and a two-dimensional detector to ensure measurements over a wide wavevector space. The scattering range is designed to vary from 2×10^{-4} to 10^{-2} Å^{-1} by changing the wavelength and/or the detector position. In order to achieve measurements over such a wide q range and keep a reasonable flux, the multibeam technique (Glinka *et al.*, 1986) was chosen for the collimation. This technique consists of using a set of masks defining several beams converging onto the detector to increase the flux at the sample position. In this paper, we describe the early measurements achieved with a prototype made of seven masks. Another original feature of this new spectrometer is a two-dimensional high-resolution image-plate detector sensitive to neutrons (Wilkinson *et al.*, 1992). Its sensitivity to γ radiation leads us to use a double-reflection supermirror monochromator instead of a velocity selector commonly manufactured from strong γ emitters. We also present the first measurements obtained with this equipment.

2. Spectrometer design

TPA is installed at the end of the cold neutron bender G5bis, the inner dimensions of the guide exit of which are 50 mm height and 25 mm width. The main constraint on the design of the instrument is the 12 m floor space available from the guide exit in the reactor guide hall. The layout of the instrument is shown in Fig. 1.

2.1. Two-dimensional position-sensitive detector

The manufacture of a large multi-detector with small pixel size (< mm) is important to achieve high-resolution SANS measurements and avoids a long length instrument, but is far from being easy. Therefore, it was decided to use a commercial image plate for X-rays (MAR345, Marresearch GmbH), equipped with a neutron converter (Gd_2O_3) and a storage imager (BaFBr doped with Eu^{2+}) read *in situ*. Such a detector allows high sensitivity and dynamics (Né *et al.*, 1993). Its dimensions are 2300×2300 pixels of 150 µm each. This definition is much higher than that of D11 at ILL, which is one of the best two-dimensional SANS spectrometers. Fig. 2 presents scattering curves from a latex–silica nanocomposite film (Oberdisse & Demé, 2002) measured on D11 and TPA (the deviation at low scattering wavevector is due to the lower q_{min} of D11 in this configuration). The detector will lie in an hermetically sealed flight tube under a helium atmosphere and will move between 1 and 6 m from the sample plane. The drawback of such detectors is their sensitivity to γ radiation, which requires special care such as the use of lead and enriched lithium (^{6}Li) neutron absorbers (instead of cadmium or gadolinium) as well as heavy concrete shielding around the detector.

2.2. Wavelength selection

A conventional velocity selector can not be used because the strong γ radiation emitted from gadolinium is not compatible with the detector. Therefore a double-reflection supermirror monochromator has been developed. It is made of two supermirrors (purchased at Swissneutronics and mounted by CILAS) with a critical angle $3\alpha_c$ (three times the critical angle of Ni) and a bandwidth around 15%. Each mirror is 30 mm high and 60 cm long, and is made from two pieces each 30 cm long glued on to a glass support.
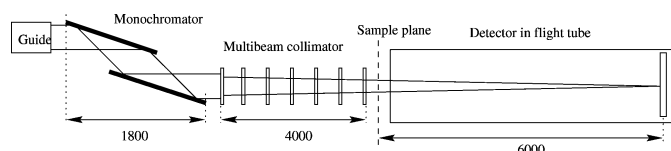

Figure 1
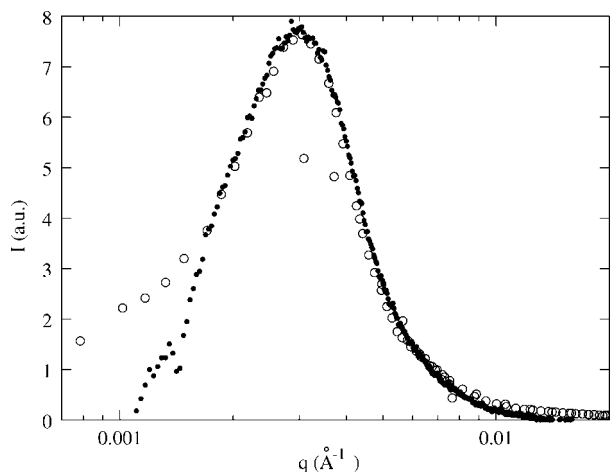Scheme of the spectrometer TPA at LLB (units in mm, drawing not to scale).

Figure 2
Scattering curves from a sample of latex–silica nanocomposite film at pH = 5 (Oberdisse & Demé, 2002) measured on D11 with a distance of 36.7 m and λ = 10 Å (open circles) and TPA with a distance of 4 m and λ = 7 Å (filled circles). Note the *q*-axis scale is logarithmic.

The characteristics of these supermirror monochromators are especially interesting for our purpose: 80% transmission, no direct view of the guide and weaker γ production. The total transmission after double reflection is therefore 64% and remains constant for all wavelengths. Fig. 3 shows the reflection curves for both supermirrors as a function of m, the critical angle normalized to that of Ni: both supermirrors have a ratio $\Delta m/m$ of 0.14.

Wavelength selection is achieved by rotation of the mirrors relative to the beam axis. Indeed, if α represents the angle between the beam axis and the mirror plane, then the reflected wavelength will be given by

$$\lambda = \frac{\alpha}{m\alpha_c}, \qquad (1)$$

with $m = 3$ and α_c, the critical angle of Ni, around $0.1°$ Å^{-1}.

The two mirrors are mounted on a rotation stage and the second one is also mounted on a 0.8 m length translation stage parallel to the beam axis in order to keep the beam axis after the monochromator fixed (with 55 mm offset relative to the original axis). This 1.8 m long monochromator is under vacuum. With this setup, the chosen
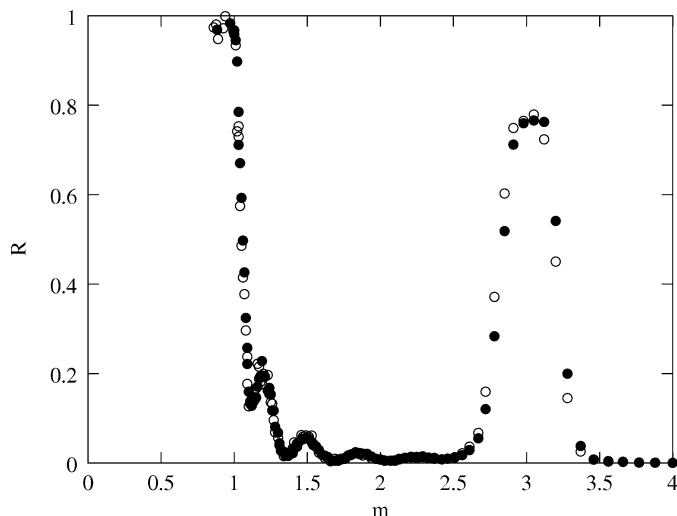
wavelength can be continuously varied from 5 to 20 Å corresponding to mirror rotations of 1.5 to 6°. Fig. 4 presents time-of-flight measurements for three different monochromator configurations. For each wavelength, $\Delta\lambda/\lambda$ equals 0.11 and is consistent with the product of the reflection curves of the two supermirrors from Fig. 3. We observe a shoulder in the peak for neutrons of wavelength 12 Å and as yet we have no clear-cut explanation of this effect. Anyway, it has negligible effect on the final resolution of the incident monochromated beam.

2.3. Multibeam collimation

The weak neutron flux on the detector area, due to the tiny collimation, the small pixel size and the inherent flux for large wavelengths, is the main limitation of this kind of spectrometer. Among the available focusing techniques, we have chosen the multibeam technique rather than a set of lenses or a focusing mirror. The use of lenses improves the intensity and gives access to lower minimum scattering vectors (Choi *et al.*, 2000) but also has drawbacks such as having to change the number of lenses when changing the wavelength. It also adds SANS from the lens material and parasitic diffusion due to surface roughness or manufacturing imperfections, and induces chromatic abberation. In the case of magnetic lenses (Oku *et al.*, 2004), 50% of the flux is already lost due to polarization. We also did not consider beam focusing with mirrors (Alefeld *et al.*, 1997) because of the large sample volumes required. Therefore, we are developing a multibeam converging collimator in order to recover reasonable incident flux. A multibeam prototype collimator of 4 m length was successfully tested. It features seven masks of 51 holes each (Fig. 5) acting as 51 beams converging on the detector plane. The neutron gain should be roughly equal to the number of beams. Each mask is made from ^{6}Li oxide powder mixed in an epoxy matrix. Their outer dimensions are 36×50 mm and 4 mm thickness. The pinholes have 1.6 and 1.0 mm diameters at the entrance and exit of the collimator, respectively. They are distributed on an hexagonal array in order to maximize their number on a given area. The distance between two consecutive pinhole centres for the entrance mask is 3.6 mm vertically and 3.2 mm horizontally. This leads to a gap of
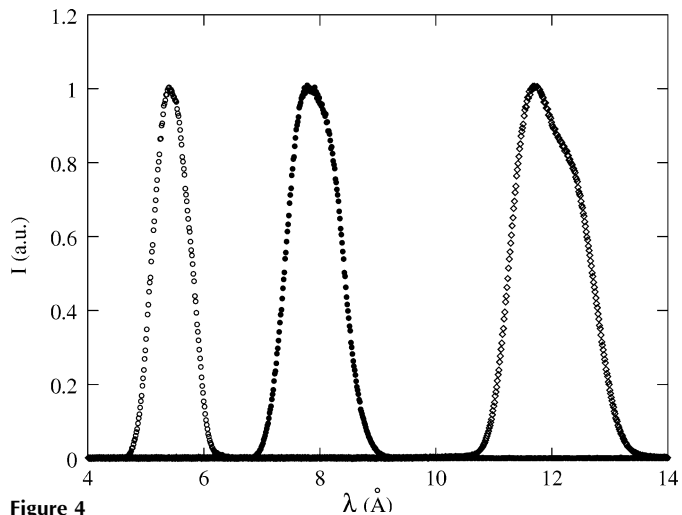

Figure 3
Typical reflectivity curve for the two-supermirror monochromator $3\theta_c$ measured on EROS (Menelle *et al.*, 2003) at LLB with an angle of 1.5°.

Figure 4
Time-of-flight measurements for neutrons of wavelength 5.4 (open circles), 8 (filled circles) and 12 Å (open diamonds). The intensities have been rescaled to unity for convenience. Measurements were made with a chopper (5 mm slit and 23 cm radius) at a rotation speed of 3000 r.p.m. and 2 mm diameter pinhole; the detector is located at 3.22 m from the chopper. The instrumental spreading is approximately 0.24 Å.
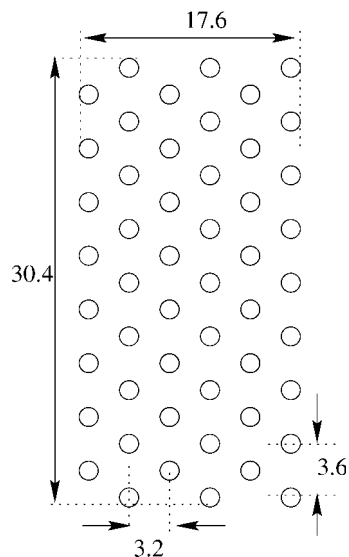
Figure 5
Representation of the pinhole geometry (units in mm, drawing not to scale) of the mask at the entrance of the collimator. The pinhole diameter is 1.6 mm.

Figure 6
Comparison of the transmitted beam intensity measured by the detector with simple (filled circles) and 16 multibeam (open circles) collimation. The entrance and exit pinhole diameters are 1.6 and 1.0 mm, respectively, and the wavelength is 7 Å. The intensity gain is 12.

2 mm between the edges of two consecutive pinholes. Since a 0.5 mm gap of matter between two neighbouring holes is close to the masks' manufacturing limit, this value will be used for the exit mask of the future collimator. Coordinates of the holes of the following masks are deduced by homothety. The number of masks required to avoid crosstalk (neutrons passing through the set of masks but not focusing onto the detector) only depends on the distance between the holes: the smaller the distance between pinholes, the higher the number of masks required. We used acceptance angle tracing (Copley, 1990) as well as *Vitess* (Zsigmond *et al.*, 2002) and *McStas* (Lefman & Nielsen, 1999) Monte Carlo simulations to show that seven masks, equally spaced, would absorb all unwanted neutrons. Fig. 6 shows the intensities obtained with the transmitted beam using the multibeam prototype with 16 pinholes and one pinhole (15 pinholes masked). The ratio between the measured intensities is 12, thus close to the expected ratio of 16 assuming the beam is homogeneous and the pinholes perfectly manufactured and aligned. The masks are mounted on a vertical stage to compensate for the neutron fall due to gravity. Indeed, a neutron of wavelength 20 Å falls 2 mm after a 4 m flight path and this value is comparable to the exit pinhole diameter of 1 mm. The masks are also mounted on horizontal stages that will act as mask changers when the detector position is changed. The final version of the collimator will be composed of three sets of masks to focus the beam at three favoured detector positions: 1, 3 and 6 m. A fourth set of masks could also be implemented with multiple slits along the vertical axis (Barker, 2006), 1.6 mm width at the collimator entrance, optimized for the 6 m detector position. These multiple slits would be used in the case of weakly and isotropically scattering samples for an improved theoretical gain of a factor of 60 compared to multiple pinholes. Although the slit-smeared intensity will undergo a different log–log slope, suitable programs allow for correct data treatment (Glatter, 1977).

3. Conclusion

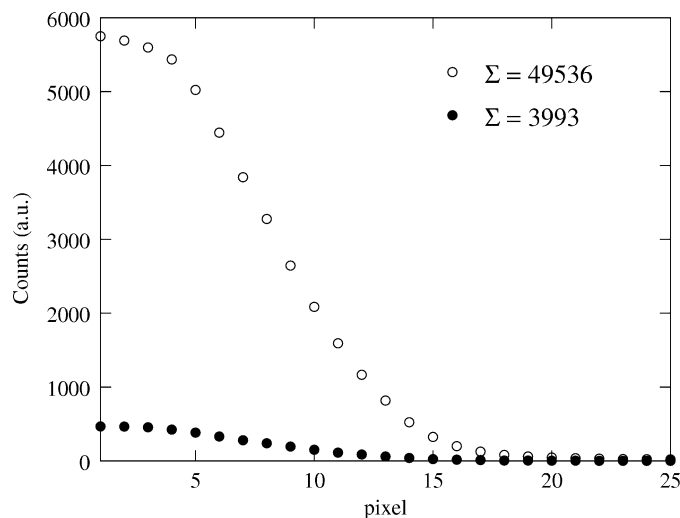The new VSANS spectrometer, TPA, already works in a non-definitive version. Its final version should give access to scattering vector magnitudes not accessible by standard SANS spectrometers, typically from 2×10^{-4} to 10^{-2} Å^{-1}. It features a newly designed double-reflection supermirror monochromator, a prototype multibeam collimator and an image plate detector.

References

Alefeld, B. C. H., Mezei, F., Richter, D. & Springer, T. (1997). *Physica B*, **234–236**, 1052–1054.
Barker, J. (2006). *Performance Review of Various Advanced Optical Designs for Very Small-Angle Neutron Scattering (VSANS) Instrumentation.* Report. NIST Center for Neutron Research, National Institute of Standards and Technology, Gaithersburg, USA.
Bonse, U. & Hart, M. (1965). *Appl. Phys. Lett.* **7**, 238–240.
Choi, S.-M., Barker, J., Glinka, C., Chang, Y. & Gammel, P. (2000). *J. Appl. Cryst.* **33**, 793–796.
Copley, J. (1990). *Nucl. Instrum. Methods A*, **287**, 363–373.
Glatter, O. (1977). *J. Appl. Cryst.* **10**, 415–421.
Glinka, C., Rowe, J. & LaRock, J. (1986). *J. Appl. Cryst.* **19**, 427–429.
Lefman, K. & Nielsen, K. (1999). *Neutron News*, **10**, 20–23.
Menelle, A., Jestin, J. & Cousin, F. (2003). *Neutron News*, **14**(3), 26–30.
Né, F., Gazeau, D., Lambard, J., Lesieur, P., Zemb, T. & Gabriel, A. (1993). *J. Appl. Cryst.* **26**, 763–773.
Oberdisse, J. & Demé, B. (2002). *Macromolecules*, **35**, 4397–4405.
Oku, T., Suzuki, J., Sasao, H., Adachi, T., Shinohara, T., Ikeda, K., Morishima, T., Sakai, K., Kiyanagi, Y., Furusaka, M. & Shimizu, H. (2004). *Nucl. Instrum. Methods A*, **529**, 116–119.
Wilkinson, C., Gabriel, A., Lehmann, M., Zemb, T. & Né, F. (1992). *SPIE*, **1737**, 324–329.
Zsigmond, D., Lieutenant, K. & Mezei, F. (2002). *Neutron News*, **13**(4), 11–14.